Icarus **148**, 370–383 (2000)
doi:10.1006/icar.2000.6466, available online at http://www.idealibrary.com on IDEAL®

Rarefied Gas Model of Io's Sublimation-Driven Atmosphere

J. Victor Austin and David B. Goldstein

Department of Aerospace Engineering, The University of Texas at Austin, Austin, Texas 78712
E-mail: victor@cfdlab.ae.utexas.edu

Received September 11, 1998; revised April 10, 2000

The circumplanetary flow of Io's SO_2 atmosphere is modeled using the direct simulation Monte Carlo (DSMC) method. This flow develops as gas sublimates from SO_2 frost in the warm subsolar region and flows toward the colder night-side, where it condenses. The axisymmetric model presented extends from the subsolar point past the terminator into the night-side. The remaining portion of the night-side atmosphere is assumed to be static. The DSMC method solves the fully viscous and compressible, non-local thermal equilibrium (non-LTE), rarefied flow problem by statistically extrapolating from the motions and collisions of representative molecules. Heating due to neutral plasma bombardment and cooling by non-LTE radiation are modeled. Quantities of a second, non-condensible gas are also added to simulate the possible effects of H_2S or O_2 in the atmosphere.

It is found that, except in the subsolar region, the flows are predominately rarefied. For high subsolar temperatures, the atmospheric flow may become supersonic and then decelerate through a diffuse, oblique shock upstream of the terminator. Appreciable local condensation occurs below the shock while the atmosphere above the shock is significantly inflated. These hydrodynamic features, among others, have implications for the observations of frost cover, atmospheric flow, and the ionosphere.

Key Words: **Io; atmospheres, dynamics; atmospheres, structure; satellites, atmospheres; satellites of Jupiter.**

1. INTRODUCTION

After more than 25 years of observation, many details of Io's atmosphere, such as its distribution, composition, pressure, temperature, and dynamics, remain uncertain. Even the dominant method of atmospheric sustenance is unclear. Models of the SO_2 atmosphere on Io are often categorized by their method of production and generally fall into one of three categories: sputtered, sublimated, or volcanic. In sputtered models, a highly rarefied, collisionally thin atmosphere is produced by the impact of energetic particles on Io's surface. Sputtering can probably be ruled out as the dominant producer of Io's day-side atmosphere by observations (Ballester *et al.* 1990, Lellouch *et al.* 1992) which suggest that Io's atmosphere is collisionally thick. Sputtering may play a significant role in the production of night-side atmosphere but will not be further considered here. Plumes of SO_2 gas provide the primary source of atmosphere in volcanic models. These models produce an atmosphere which is spatially nonuniform, ranging from highly collisional near the source to collisionless elsewhere. We have discussed preliminary results of a rarefied gas model of volcanoes on Io in a previous publication (Austin and Goldstein 1996) and will later expand on that work in a subsequent companion to the present paper.

Here we discuss a model of the sublimation/condensation-driven atmospheric flow on Io. Sublimation models consist of an SO_2 atmosphere that is controlled by the vapor pressure of SO_2 surface frost. The gas sublimates from SO_2 frost in the warm subsolar region where the vapor pressure is high and flows toward the colder night-side, where the vapor pressure is low and the flow condenses. The acceleration of the flow due to this vapor pressure difference and cooling due to expansion can cause the flow to become supersonic. Sublimation models yield an atmosphere which ranges from collisionally thick at the subsolar point to collisionless on the night-side.

Io's atmosphere was first detected by the radio occultation experiments of Pioneer 10, which probed the ionosphere near the terminator. Kliore *et al.* (1975) used these data to calculate an atmospheric surface pressure on the order of 1 nbar near the terminator. SO_2 gas was first detected by Pearl *et al.* (1979) using the Voyager IR spectrometer (IRIS) to identify SO_2's ν_3 band at 7.3 μm. The measurement was made near Loki Patera, and Pearl *et al.* (1979) assumed a gas temperature of 130 K, which led to a surface pressure of 100 nbars. Lellouch *et al.* (1992) later reinterpreted the same IRIS data but included non-LTE effects to find surface pressures in the range 5 to 40 nbar. The UV spectrum observations of Ballester *et al.* (1994) are best fit by a cool gas with large extent, and hence lend support to a sublimated atmosphere. However, the millimeter-wave observations of SO_2's 222-GHz rotational line by Lellouch *et al.* (1990) are best fit by a warm gas with limited extent and so are best matched by the volcanic models (Lellouch *et al.* 1992). The observations of McGrath *et al.* (2000) affirm that Io's atmosphere is likely controlled by both sublimation and volcanic influences: their spatial trend of SO_2 column density with latitude agrees well with our sublimation model, yet, consistent with volcanic models, they find higher densities over the plume Pele.

0019-1035/00 $35.00

Ingersoll *et al.* (1985) modeled the sublimation-driven circumplanetary flow around Io by solving the vertically integrated conservation equations in one dimension. They assume that the frost temperature is subject to a simple radiative balance, that the atmospheric flow is turbulent, and that Io's rotation is unimportant. They find that in the process of expanding away from the subsolar point, the flow pressure and temperature drop and that the Mach number may reach 4. In a second paper Ingersoll (1989) modifies his earlier work to account for nonuniform surface properties found in observational studies. Local volcanic plumes and patchy frost cover are handled. Several flows in simple geometries are solved analytically, albeit with many assumptions. In particular, the turbulent flow assumption is dropped in favor of an inviscid model with mean flow velocity lost through the evaporation and condensation processes. Moreno *et al.* (1991) simulated an atmosphere of sublimed SO_2 frost as well as day- and night-side volcanic atmospheres using a time-explicit, finite-volume formulation of the equations of inviscid, compressible gas dynamics that incorporated a crude radiative transport model. In common with Ingersoll (1989), they find that non-condensing flow over a hot dry surface travels much further than does condensing flow over a cold surface. Wong and Johnson (1995) used a similar inviscid, finite-difference model to simulate a sublimation-driven Ionian atmosphere with the addition of plasma bombardment, UV heating, and IR cooling. Wong and Johnson (1996) improved upon their previous model by adding viscous terms (in the vertical direction only), Joule heating, and non-LTE cooling. They find that plasma bombardment significantly inflates the atmosphere on the trailing side of Io, such that their SO_2 column densities are about an order of magnitude greater than that observed by McGrath *et al.* (2000). Wong and Smyth (2000) used essentially the same model as Wong and Johnson (1996) but increased the plasma heating through both a higher ion flux and by reaccelerating the ions after collisions. As would be expected from the increased heating, they find an even hotter, more inflated atmosphere than the colder model.

As indicated in the above discussion, previous modeling of Io's sublimation-driven atmospheric flow has neglected certain important flow features. These features include viscous and rarefaction effects as well as effects of non-LTE. We begin the present work with a brief discussion of the computational method since its application to a full planetary atmosphere is relatively unique (Austin and Goldstein 1997, Marconi *et al.* 1996, Combi 1996). We examine certain important computational issues and detail the representation of the gas model and boundary conditions. We then present results in which the effects of surface temperature, plasma heating, and non-condensible species are explored.

2. MODEL

At a subsolar temperature of $T = 115$ K the local mean free path ($\lambda \cong [\sqrt{2}\pi d^2 n]^{-1}$, where $d = 7.16 \times 10^{-10}$ m is the nominal diameter of a gas molecule and n is the number density) at the surface is about 5 m while the pressure scale height ($H = RT/g$, R is the gas constant and g is the gravitational acceleration on Io) is about about 7.2 km, so it would at first appear that rarefaction is not greatly important. However, n drops exponentially with both altitude and solar zenith angle, θ, so regions of rarefied flow occur at modest altitudes and θ. For example, as will be shown below, an atmospheric shock was found to form at about $\theta = 63^\circ$ for certain input conditions. Just upstream of the shock λ ranges from about 340 m at the surface to 4 km at 20 km altitude where the Mach number is highest.

In contrast to the work of Ingersoll *et al.* (1985), the present work assumes viscous, laminar flow. Ingersoll *et al.* (1985) argued that the Reynolds number based on H and surface density was of order 10^5 over most of the flow for the case of $T_{\text{subsolar}} = 130$ K. However, much of the dense atmosphere which might sustain turbulent flow lies at low altitude and small values of θ where there is little flow velocity. For a nominal situation of $T_{\text{subsolar}} = 115$ K, the peak Reynolds number ($\text{Re} = |V|h\rho/\mu$) occurs near $\theta = 25^\circ$ and about 5 km altitude and is approximately 200—a value where laminar flow almost assuredly exists ($|V|$, h, ρ, and μ represent the local flow speed, altitude, density, and viscosity). Moreover, both the favorable pressure gradient over the entire region of interest and the boundary layer suction due to surface condensation below the higher speed flow promote boundary layer stability.

2.1. The DSMC Method

In low-density flows the Navier–Stokes equations break down because the scale of the gradients of the flow variables becomes comparable to the mean free path. A rarefied gas dynamics technique is required to accurately model these flows. The direct simulation Monte Carlo (DSMC) method is well suited to simulating much of Io's atmospheric flow because it can handle rarefaction, mixtures of gases, thermal non-equilibrium, gravity fields, variable molecule/surface adhesion coefficients, and radiative heat transfer.

The DSMC method efficiently models low-density gas flow by simulating the movement and collisions of millions of representative particles. By using a time step smaller than the mean time between molecular collisions, the movement of the molecules can be effectively decoupled from the collisions. During a time step the representative molecules are first moved appropriately to their stored velocities and then pairs of nearby molecules are randomly chosen to collide, resulting in new velocities. The variable hard sphere model (Bird 1994), in which the collision cross sections vary with the relative collision velocity, was used to obtain the SO_2 viscosity $\mu = 1.164 \times (T/T_{\text{ref}})^{1.05}$ N s m^{-2}, where $T_{\text{ref}} = 273$ K (Chapman and Cowling 1970). Periodically during the calculation the simulated molecule properties are sampled so that the macroscopic flow quantities can be calculated and exported.

The modern DSMC approach, which is the most widely used method for computing complex, rarefied flows of engineering

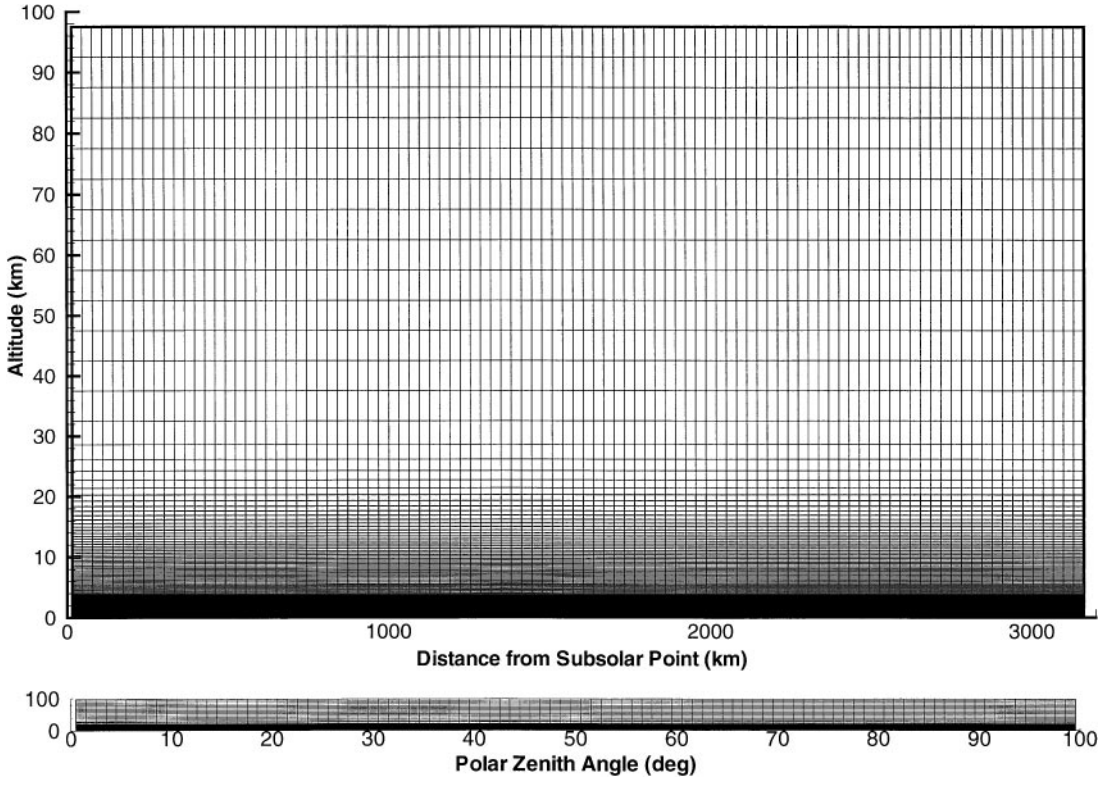

FIG. 1. Computational grid used for simulations at $T_{\text{subsolar}} = 115$ K. The grid is 200 cells high by 200 cells wide. The cells are 100 m high at the surface and grow exponentially with altitude. Above 30 km in altitude the cells are limited to a height of 5 km. Horizontal cell spacing is approximately 16 km. The upper figure has been stretched in the vertical direction. The lower figure shows the grid at the correct aspect ratio.

and scientific interest, is described by Bird (1994). That approach has been expanded for the present effort. Our modifications include the inclusion of a constant gravitational body force so the molecules follow parabolic trajectories, the introduction of an adaptive weighting factor distribution and collision limiters to handle the huge density variations, the use of a novel semi-structured grid as well as a multi-grid approach to enhance spatial resolution, the development of non-LTE radiation and cold plasma impact models suitable for planetary atmospheres, and the use of progressive ensemble averaging to speed the approach to steady state. A more detailed description of the methodology is given in Austin and Goldstein (1999).

2.2. *Geometry*

The computational model uses a two-dimensional, cylindrical geometry which is axisymmetric about the subsolar point. The height of the cylinder corresponds to the altitude above the surface of Io and the radius corresponds to the distance along the surface from the subsolar point (or, equivalently, the solar zenith angle, θ). This plane-parallel geometry (essentially a flattened hemispherical shell) is valid because the height of the hydrodynamic region of the atmosphere is small compared to the radius of Io. Results obtained using this model have been found to agree well with a spherical domain but at a considerable savings in computational cost. The horizontal (or radial) velocity of the gas (positive away from the subsolar point) is designated as U while V is the vertical velocity.

An example grid is shown at the top of Fig. 1. Through most of the domain, the cells are exponentially spaced in the vertical direction so that their height is proportional to the local mean free path. Grids for higher subsolar temperature simulations use smaller cells at the surface than lower temperature simulations due to the higher vapor pressures and smaller mean free paths. High vertical resolution is necessary at low altitudes because there are large property gradients (density, velocity, temperature, etc.) across the boundary layer. At higher altitudes, the growth of the cell heights is limited so that they remain small when compared to the scale height. The width of the cells in the horizontal direction has a much larger spacing of approximately one-half a polar degree as horizontal property gradients are generally much weaker. Enhanced horizontal resolution is used, however, to resolve regions containing large gradients or atmospheric discontinuities (within the shock, for example). Regardless of our *a priori* assumptions about the nature of the grids required to capture the flow features of interest, we performed many grid resolution studies using progressive grid refinement to assure spatial convergence. Note that in the figures to be shown later only a portion of the computational domain is shown and the scales have been magnified in the vertical direction to allow

details to be seen. For comparison, the bottom of Fig. 1 shows the full domain with the correct aspect ratio. Also shown is the corresponding solar zenith angle, θ, along the x-axis.

2.3. Boundary Conditions

Particular emphasis has been placed on utilizing a suitable representation of the gas/surface interface. Experimental results indicate that for a normal rough surface the sticking coefficient, α, for SO_2 gas on SO_2 ice is expected to be approximately one (S. Loyalka, private communication, 1998). Thus, we model a surface on which every impacting SO_2 molecule condenses. This allows a free molecular flow to virtually pour into the surface unimpeded while a higher density flow is buffered from the surface by sublimated gas. Previous calculations (Ingersoll *et al.* 1985, Ingersoll 1989, Moreno *et al.* 1991, Wong and Johnson 1995) have modeled the influx as proportional to the difference between the local surface vapor pressure and the near surface atmospheric pressure. This is only valid in the fully continuum regime where the inflowing, condensing gas can equilibrate with the outflowing, sublimating gas before condensing on the surface. In more rarefied conditions, such as those which exist on Io away from the subsolar region, the flow is quite rarefied and the condensing gas can pass through the sublimating gas to the surface without equilibrating.

The sublimation rate of SO_2 molecules used here is given by

$$N_{\text{sublimated}} = P_{\text{vapor}}/\sqrt{2\pi k T_{\text{surface}} M_{SO_2}}, \quad (1)$$

where the equilibrium vapor pressure (in pascals) is (Ingersoll *et al.* 1985)

$$P_{\text{vapor}} = 1.52 \times 10^{13} e^{-4510/T_{\text{surface}}}, \quad (2)$$

the surface temperature (in K) determined by radiative balance is (Ingersoll *et al.* 1985)

$$T_{\text{surface}} = (T_{\text{subsolar}} - 50) \times \cos^{1/4}\theta + 50, \quad (3)$$

k is Boltzmann's constant, and M_{SO_2} is the molecular mass of SO_2. Sublimated molecules are emitted with a proper normal velocity distribution and an internal rotational energy drawn from a Boltzmann distribution corresponding to T_{surface}.

The right–hand boundary ($\theta = 100^\circ$) is modeled as a specularly reflecting wall. There the cylindrical geometry used is decidedly unphysical because it continues to expand as θ increases beyond 90° while the width of a true slice of a spherical domain reaches a maximum and then begins to contract. However the cold surface near the terminator is such a strong sink that the gas flowing from the warmer regions does not advance beyond about 80°. The specular boundary condition is used to maintain a uniform profile of low-density background gas which is assumed to exist over the cold night side. The wall has been placed at a sufficient distance, however, such that it has no effect on the flow. This is checked by comparing the pressure along the wall to an isothermal profile at the local night side surface temperature.

The boundary conditions for the remaining two sides of the domain are trivial. The upper boundary represents a vacuum—any molecules which strike the top of the domain are removed from the calculation; such events are extremely rare. No boundary condition is needed for the left side of the domain ($\theta = 0^\circ$) since it is the axis of symmetry.

2.4. Initial Conditions

The present paper concentrates on the quasi-steady atmospheric flow. However, the DSMC method must reach steady state via an integration in time from a presumed initial condition and this process consumes a large fraction of the computational effort. During the relaxation from the initial condition to steady state a time step much greater than the mean collision time is used. This large step allows the calculation to proceed quickly but results in an excessively long mean free path and hence an overly viscous fluid. Once a steady flow has been obtained, the time step is reduced and the model is relaxed to steady state again. The relaxation time is small (usually <1000 time steps) because the flow can quickly equilibrate with the surface. This procedure is repeated until the time step is smaller than the mean collision time over most of the flow, which is the limiting condition for the DSMC method.

Two different initial conditions are used depending on the model configuration. When only SO_2 is being modeled, the initial condition is to simply start with no atmosphere at all and allow the frost to sublimate until a steady atmosphere forms (this is equivalent to the unsteady flow which develops when the surface of Io is quickly warmed after passing out of Jupiter's shadow). When a non-condensible gas is also being modeled, we start the calculation at time zero with a hydrostatic, isothermal atmosphere at the local surface temperature and let the atmosphere relax to steady state from there.

Although this paper concentrates on steady state atmospheric flow we note that interesting transient flows were observed during the unsteady startup. In particular, in starting from an initial vacuum with a large amount of plasma heating (discussed in the following section), it was found that the gas which first sublimates "blows up" and rapidly expands out of the domain before the flow settles down to the expected steady state. This may be a result of the plasma energy passing all the way to the lower atmosphere (since the upper atmosphere—which normally absorbs the plasma energy—has not been populated with gas yet) to be absorbed by the dense gas which sublimates from the surface near the subsolar point. We plan to investigate this transient further and explore whether it could be a factor in the "flash" which has occasionally been observed (Nelson *et al.* 1993) when Io passes out of Jupiter's shadow.

2.5. Plasma Heating

Heating due to bombardment from the plasma co-rotating with Jupiter's magnetic field is modeled using a modification of the time-splitting method already used in the DSMC calculation.

An additional step is added during which plasma energy is introduced into the flow. The absorption of plasma energy is integrated cell-by-cell from the top of the domain down to the surface in each column of cells. During this integration the gas flow field is held frozen; i.e., the gas is assumed to be cold compared to the plasma. Since the velocity of the plasma particles (approximately 60 km sec^{-1}, Strobel *et al.* 1994) is much greater than that of the average atmospheric gas molecule ($\frac{1}{2}kT \sim 0.2$ km sec^{-1}, where T is the gas temperature) the solution can be effectively decoupled in this manner. Currently the plasma particle momentum is not transferred to the atmospheric particles and vibration, dissociation, and electronic excitation are neglected.

Only a fraction of the total energy of the incident plasma molecules is assumed to be effective in heating Io's atmosphere. We use an effective plasma energy of 1.3 erg cm^{-2} sec^{-1}, which is consistent with Wong and Johnson (1995) and Lellouch *et al.* (1992). The energy deposited in each cell is given by

$$E_{\text{deposited}} = E_{\text{in}} \times (1 - e^{-\sigma N h_{\text{cell}}}), \tag{4}$$

where N is the number density and h_{cell} is the height of the cell. The cross section, σ, for collisions between plasma particles and SO_2 molecules is assumed to be 1×10^{-16} cm^2, which was used by Lellouch *et al.* (1992). Others have used larger values of σ (Wong and Johnson 1995, Strobel *et al.* 1994) which lead to greater energy deposition at high altitudes. E_{in} is the plasma energy entering the top of each cell in each time step and is equal to the energy entering the top of the atmosphere less any energy lost in higher cells. The energy deposited in a computational cell is evenly divided among all the molecules in the cell and is further evenly divided between the translational and rotational energy modes (assuming a local equilibrium distribution). In this model the plasma flux impinges on the atmosphere vertically over the whole domain. As such, this geometry corresponds to Io at western elongation and is only truly correct near the subsolar point where the plasma impingement is normal to the surface. However, farther away from the subsolar point, where the slant path of the plasma impingement is significant, the gas is collisionally thin, so the results should be relatively insensitive to the plasma path.

Heating from solar UV radiation was not modeled; however, as indicated in the following discussion, its effects are expected to be small when compared to plasma heating. Lellouch *et al.* (1992) obtain a heating per molecule of gas due to solar UV of 2.9×10^{-17} erg sec^{-1} which is roughly an order of magnitude less than the plasma heating above and at the exobase in our model. Likewise, Wong and Johnson (1995) find that the effect of the plasma is much larger than that due to UV heating at high altitudes. Below the exobase the heat transfer in the gas is dominated by conduction and convection to the surface. The UV heating of a column of gas is significantly less than the heat transfer between the gas and the surface in most areas of the flow. Strobel *et al.* (1994) observe that radiative heating is "quite small" below 70 km in their model.

2.6. Radiative Cooling

We model the non-LTE IR cooling of SO_2 from its rotational internal energy. The cooling is based on the simplified model of Lellouch *et al.* (1992) which assumes an optically thin gas everywhere. As such, radiative cooling is applied everywhere in the domain. Lellouch *et al.* (1992) give the cooling rate per molecule as $R = 4\pi \sum_j B_{\nu_j} S_j$, where B_ν is the Planck function and S_j is the strength of the jth rotational line. In our model we use the effective rotational temperature of each molecule to calculate its radiative cooling rate and then remove the energy from its rotational energy. This allows us to model the non-LTE cooling which occurs in the non-continuum regions of the atmosphere (high in altitude and far from the subsolar point).

2.7. Noncondensible Background Gas

Molecules of O_2 and H_2S at various gas pressures were added to study the effect of the presence of a gas that is non-condensible at the expected surface temperatures. Any non-condensible molecules which collide with the surface are diffusively reflected with the appropriate surface temperature assuming full thermal and momentum accommodation.

3. RESULTS

The parameter space one can explore is broad. Hence, rather than examine the full space, we examine a baseline case and then vary one parameter at a time. We consider our baseline case to be that of a fully frost covered Io with only SO_2 gas present. The subsolar frost temperature is 115 K and there is no plasma heating or radiative cooling. Contours of the hydrodynamic properties are seen in Fig. 2. SO_2 vapor sublimates from the subsolar region ($\theta < \sim 32^\circ$) and condenses elsewhere. The flow streamlines illustrate the overall flow. Along the symmetry axis the flow is vertical and of low speed. As θ increases, the flow speed increases and becomes nearly horizontal as the gas is driven by the strong horizontal pressure gradients. The results show noise at high altitudes due to the statistical nature of the DSMC method. The statistical noise is proportional to the inverse square root of the sample size of independent particles in each computational cell. Because of the density gradient, this sample size decreases exponentially with altitude. The noise is a common feature of DSMC calculations and does not affect the results. The cell sizes and the number of computational particles were chosen to restrict the higher noise to regions where the flow is collisionless.

A most prominent flow feature is a strong atmospheric discontinuity near the terminator. The discontinuity is oblique and curved due to the non-uniform incoming flow; the sonic line, which marks the presence of the actual discontinuity, parallels the surface until about $\theta = 68^\circ$, where it turns up to an inclination of about 27°. We term the discontinuity a shock wave at low altitude because it is abrupt and because nearly all of the gas descends immediately downstream from the shock. The vapor downstream of the shock is super-saturated with respect

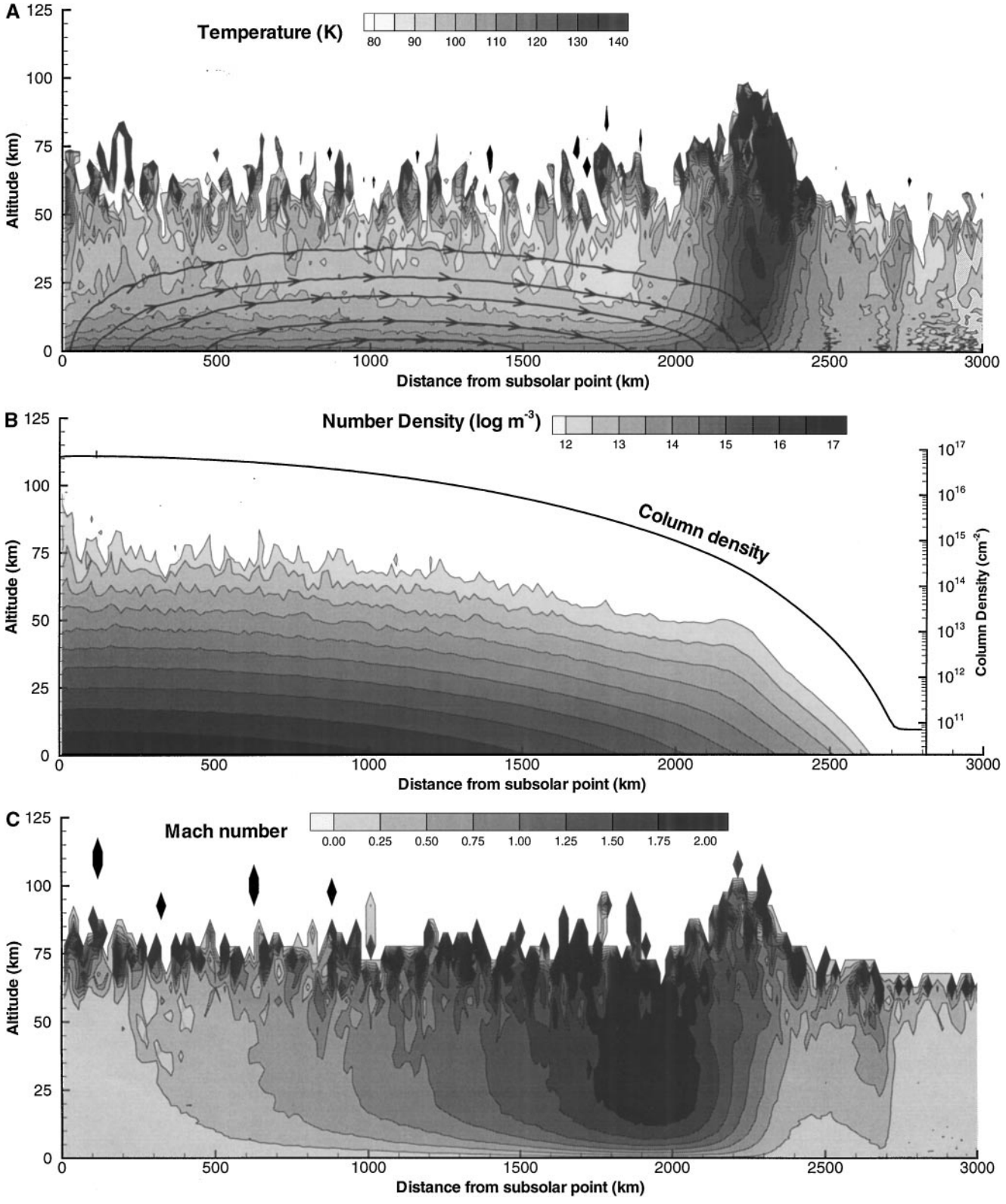

FIG. 2. Contours of temperature (A), number density (B), and Mach number (C) for a sublimation-driven atmosphere with $T_{\text{subsolar}} = 115$ K. Streamlines are included on the temperature plot. The noisiness of the results is due to the statistical nature of the DSMC method and is greater in the upper part of the domain (above 60 km) where there are few computational particles.

to the surface vapor pressure and the atmosphere collapses toward the surface as the near-surface vapor condenses. At higher altitudes, however, the gas just downstream from the discontinuity expands upward (into space) in a manner more like what one expects from a hydraulic jump. A hydraulic jump is an open-channel flow phenomenon which occurs when the flow is supercritical (the flow speed is greater than the wave speed). Information cannot propagate upstream, so the flow must change through an abrupt jump in depth involving turbulent mixing. Tidal bores are a common example of a hydraulic jump. The expansion is at this point a rarefied effect in that it occurs only above an altitude of about 60 km, where λ is in excess of 1000 km. The gas, which is shocked (and thus warmed to about 120 K) by collisions at lower altitudes, expands ballistically upward, creating an inflated atmosphere in the region of the discontinuity from about $\theta = 65^\circ$ to 75°, as can be seen in Fig. 2B. This inflated atmosphere could help explain the radio-occultation results of Pioneer 10 (Ingersoll 1989) and Galileo (Hinson *et al.* 1998).

Figure 3 provides a distribution of Bird's breakdown parameter (Bird 1994), $P_B = \frac{\partial \rho}{\partial x} U/\rho\eta$, which indicates regions where rarefaction is important. Here η is the collision rate. Rarefaction must be considered where P_B exceeds approximately 0.02. Also shown is the commonly used Knudsen number $\mathrm{Kn} = \lambda/H$; for values of Kn greater than 0.1, rarefied effects become important. Clearly the region at low altitude near $\theta = 0$ is in equilibrium as the density is high and flow gradients are low. Elsewhere, however, the density is low and rarefied effects should be expected. In the shock region, in particular (indicated by the superimposed contours of a measure of thermal non-equilibrium $T_{\mathrm{trans}} - T_{\mathrm{rot}}$), the gas is not in equilibrium. Hence, one expects a rather thick shock and, as seen, the shock is nearly 200 km thick (or about 15 scale heights) at 20 km altitude. Further evidence of the non-equilibrium nature of the flow is seen in Fig. 4, which indicates velocities and Mach numbers right at the surface. Using a continuum flow assumption, the velocity tangent to the surface would be zero (no-slip). In the present case, however, the U velocity at the surface rises to tens of meters per second due to rarefied slip. The surface Mach number reaches almost 0.45 below the foot of the shock as the high speed flow is driven into the surface by the relatively high pressure behind the shock.

Figure 4 illustrates the nature of the rarefied boundary layer: as the velocity at altitude increases so does velocity slip near the surface. Also note that the viscous boundary layer is well resolved by at least 10 grid sites (Fig. 4B). If we compute a friction velocity as $u^* = \sqrt{\tau_w/\rho}$ and a friction length scale, $l^* = \nu/u^*$, we find that the cell height remains less than l^*. Here τ_w is the wall shear stress, $\mu du/dy$, and ν is the kinematic viscosity. The atmospheric density and pressure are largest at low altitude near $\theta = 0$ and fall off with altitude and solar zenith angle. Most of the decrease with θ is due simply to the reduced surface temperature (Eq. (3)) rather than to the gas dynamics associated with the expansive flow away from the subsolar point.

A range of subsolar temperatures was investigated using the model. The acceleration of the flow, peak Mach number, and strength of the shock were found to vary greatly with the subsolar temperature. Figure 5 shows temperature contours for a range

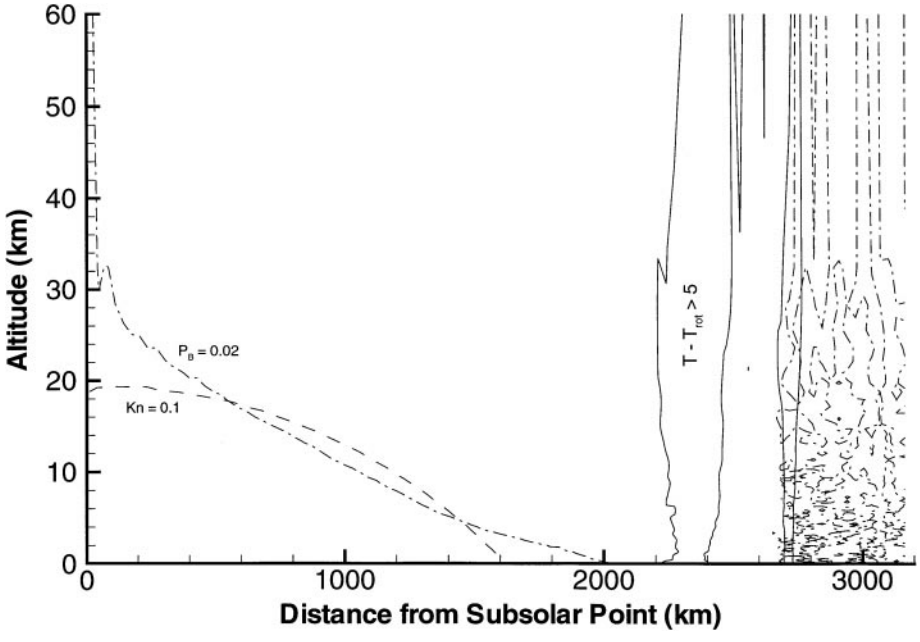

FIG. 3. Rarefaction parameters and a rarefied effect. Shown are the values of Knudsen number (Kn) and Bird's breakdown parameter (P_B), which indicate the transition from continuum to rarefied fluid dynamics. The area above and to the right of the curves would be expected to show rarefied effects. An example of a rarefied effect is seen in the region marked "$T - T_{\mathrm{rot}} > 5$," where the effective rotational temperature of the gas molecules differs from the translational temperature by more than 5 K.

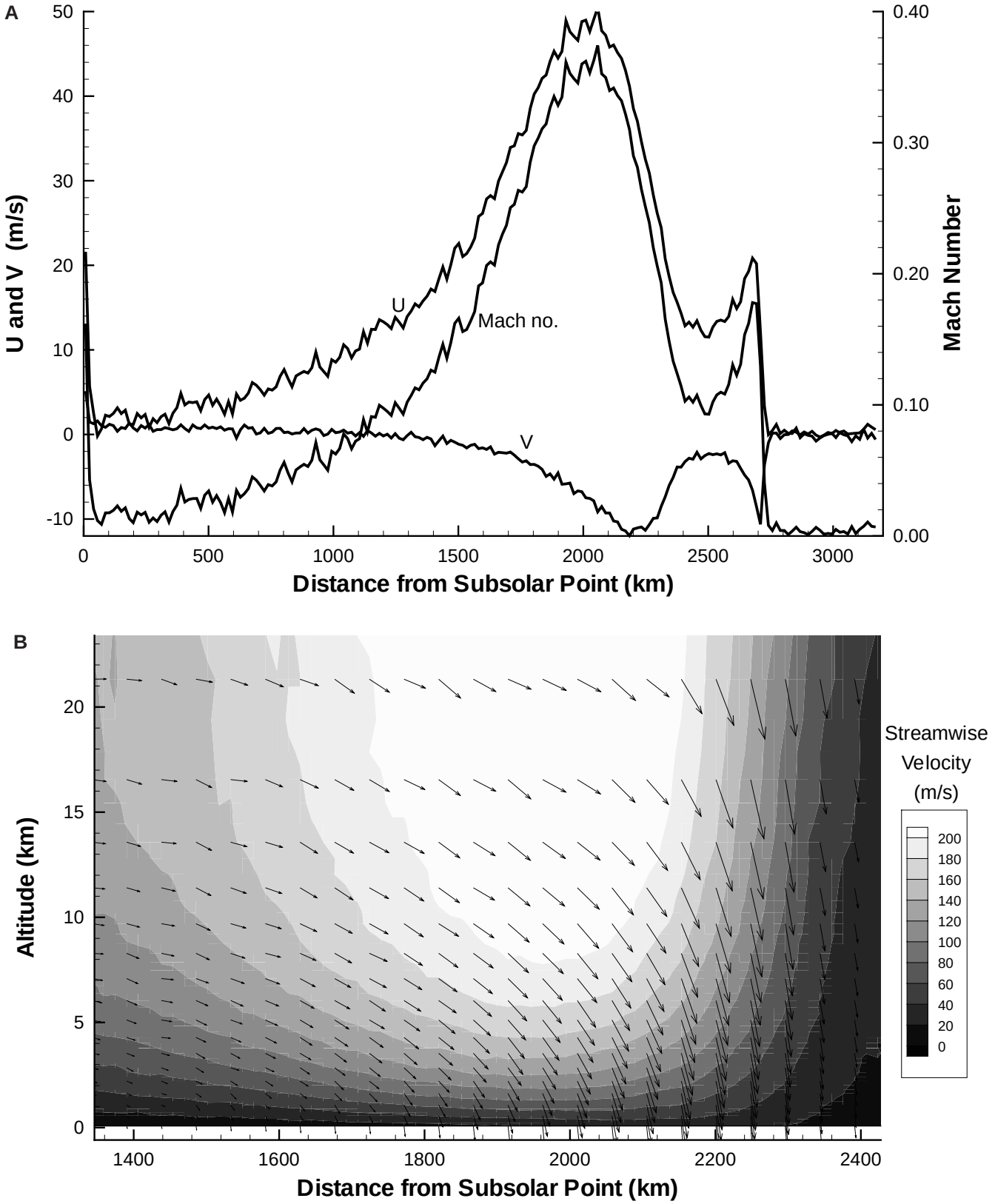

FIG. 4. Rarefied boundary layer dynamics. (A) U (horizontal) and V (vertical) velocities and Mach number along the surface, showing the velocity slip due to rarefaction and the dramatic flow changes through the shock at around $x = 2200$ km. (B) Closeup of the near surface region below the shock showing streamwise velocity contours and velocity vectors. Only one vector is drawn for every nine cells.

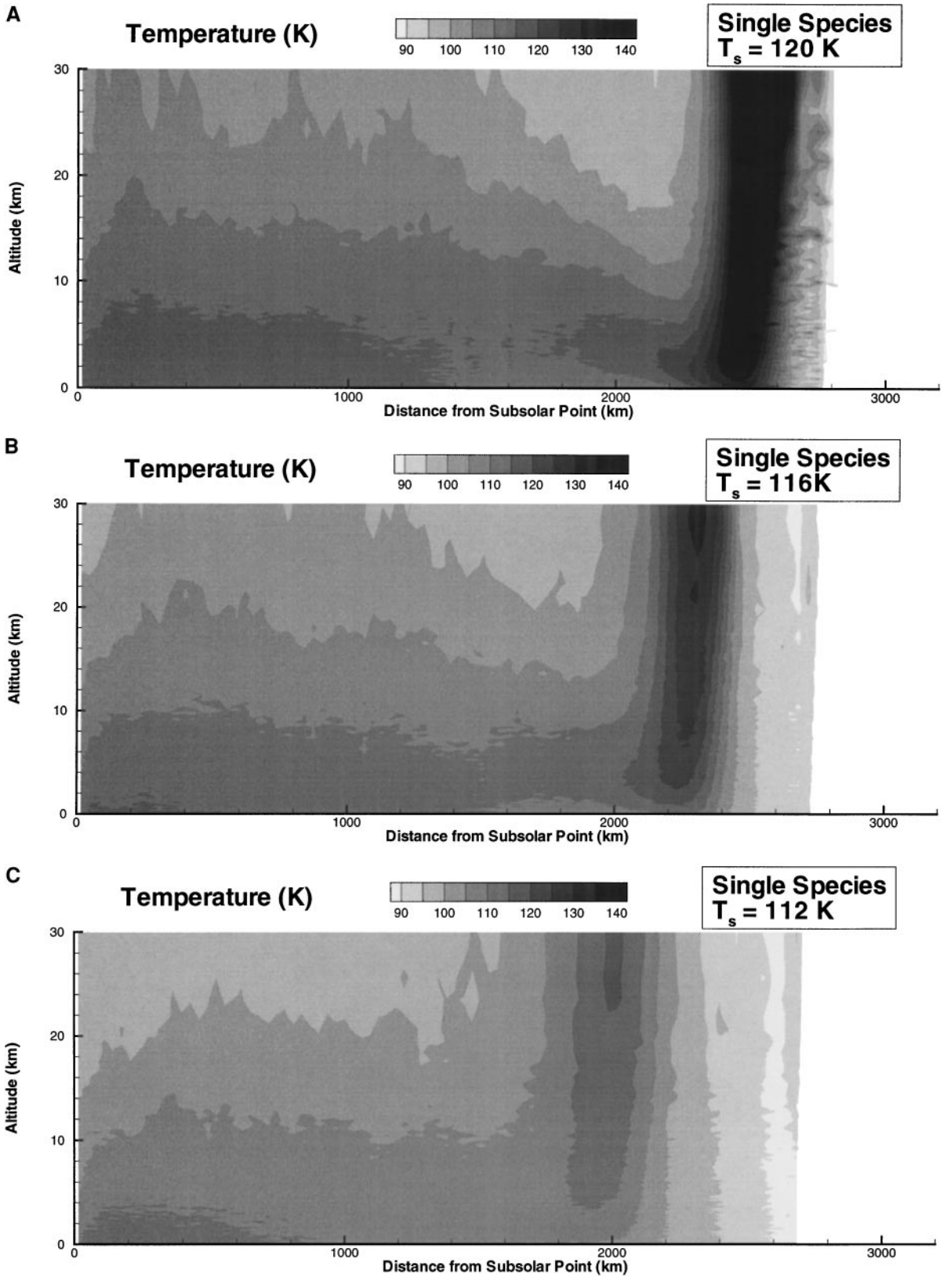

FIG. 5. Temperature contours showing the relative strength of the shock for (A) $T_{\text{subsolar}} = 120$ K, (B) $T_{\text{subsolar}} = 116$ K, (C) $T_{\text{subsolar}} = 112$ K. The vertical temperature gradients upstream of the shock remain weak. The shock moves downstream as T_{subsolar} is increased.

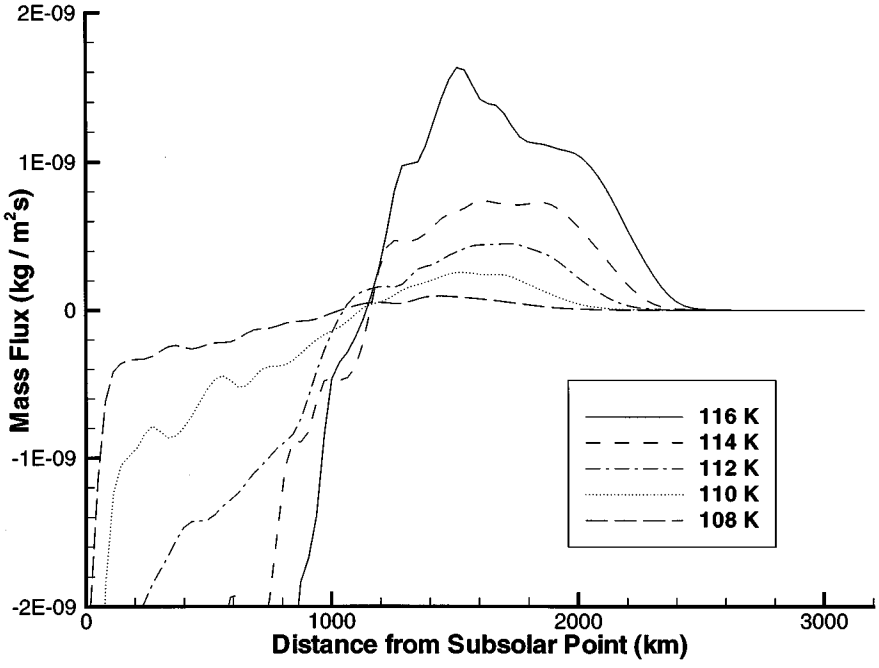

FIG. 6. Mass flux due to condensation/sublimation at the surface for several subsolar temperatures. Negative values denote flow out of the surface (sublimation) and positive values denote flow into the surface (condensation).

of subsolar temperatures from 112 to 120 K. The progression of plots shows that as the subsolar temperature increases, the shock becomes stronger and moves farther away from the subsolar point. The peak Mach numbers increase with T_{subsolar} to reach a value of $\sim$2.2 at $T_{\text{subsolar}} = 120$ K. Even at such a high speed, the peak Reynolds number is still only 260 and the flow should remain laminar.

The shock strength also has a significant effect on the surface deposition pattern of SO_2 frost. Figure 6 shows the net mass flux per unit time at the surface for different subsolar temperatures. Note the bump in the deposition pattern for the two warmest curves (approximately 2000 km from the subsolar point) which represents increased condensation just below the shock. The nature of such flows may be determined by observing the patterns of frost deposition caused by the condensing gas. These patterns may occur at high latitudes or around large frost patches. The deposition patterns may be partially or fully washed out in the east–west direction due to the rotation of the subsolar point as Io orbits but should remain in the north–south direction. The multiple-humped pattern of mass deposition rates shown indicates that a banded pattern of surface frost might be expected. These patterns are localized to the shock and are distinctly different from the global pattern that Moreno *et al.* (1991) describe.

Next, plasma heating and IR cooling (as described in Sections 2.5 and 2.6) were added to the model. The Plasma heating was found to significantly alter the thermal structure of the upper atmosphere and affect the nature of the terminator shock. Figure 7 illustrates the same quantities with plasma heating and IR cooling as Fig. 2 did for the baseline case. The atmospheric flow carries most of the plasma-heated gas away from the subsolar region towards the terminator. The gas reaches its maximum temperature (240 K, versus 120 K for the case without heating) just before the shock. After falling through the shock, the gas cools due to conduction to the ground and then condenses. The plasma heating also causes a significantly more inflated atmosphere (Fig. 7B comparated to Fig. 2B) with much higher gas pressures at altitude. The standing shock does not curve upward as in the unheated case and instead extends from the ground at at a roungly constant 5° angle. The gas over the night-side is only slightly warmed by the plasma and remains stationary.

We finally consider the effects of a second species which is non-condensible at the temperatures expected on Io. Both H_2S, a common volcanic gas, and O_2, a stable product of the photodissociation of SO_2, were used as the non-condensible species. The data presented here are for O_2, but results using H_2S were similar. Figure 8 shows the concentration of SO_2 relative to O_2 with velocity vectors overlaid. For these cases the simulated surface pressure of O_2 on the night-side (on the far right of the figure) ranges from 10^{-8} Pa (lowest figure) to 10^{-6} Pa (upper figure). The non-condensible gas clearly halts the advance of SO_2 toward the night side behind a sharp species discontinuity. The SO_2 neither overflows nor underflows the second species but simply pours into the ground just after the shock. The higher the back pressure of non-condensible gas, the less the SO_2 gas is able to penetrate toward the night-side. However, it can be seen in Fig. 9 that for the range of pressures that were studied, the non-condensible gas has a negligible effect on the SO_2 deposition

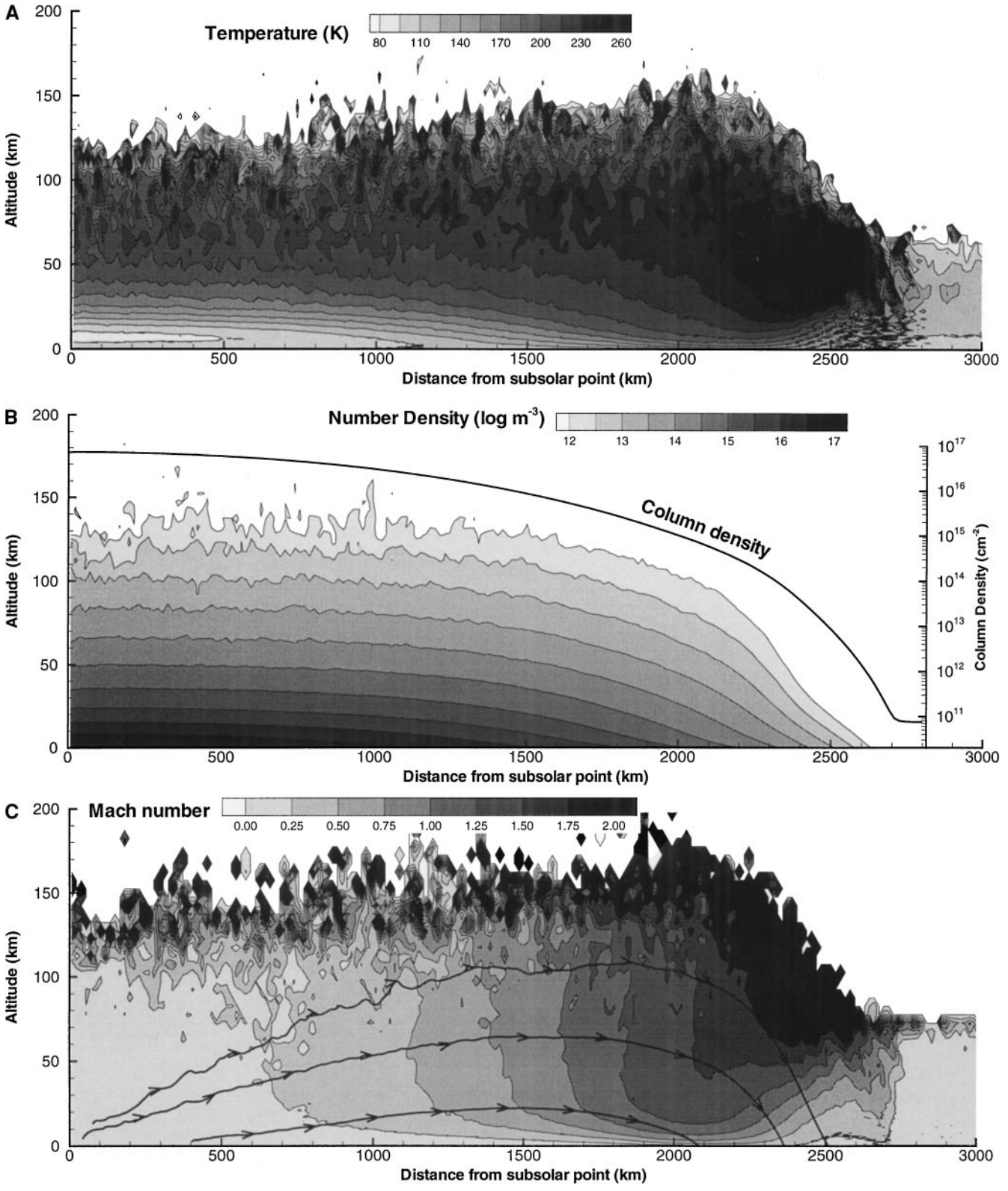

FIG. 7. Contours of temperature (A), number density (B), and Mach number (C) for the same conditions as those in Fig. 2 ($T_{\text{subsolar}} = 115$ K) but including plasma heating and non-LTE IR cooling. Streamlines are included on the Mach number plot.

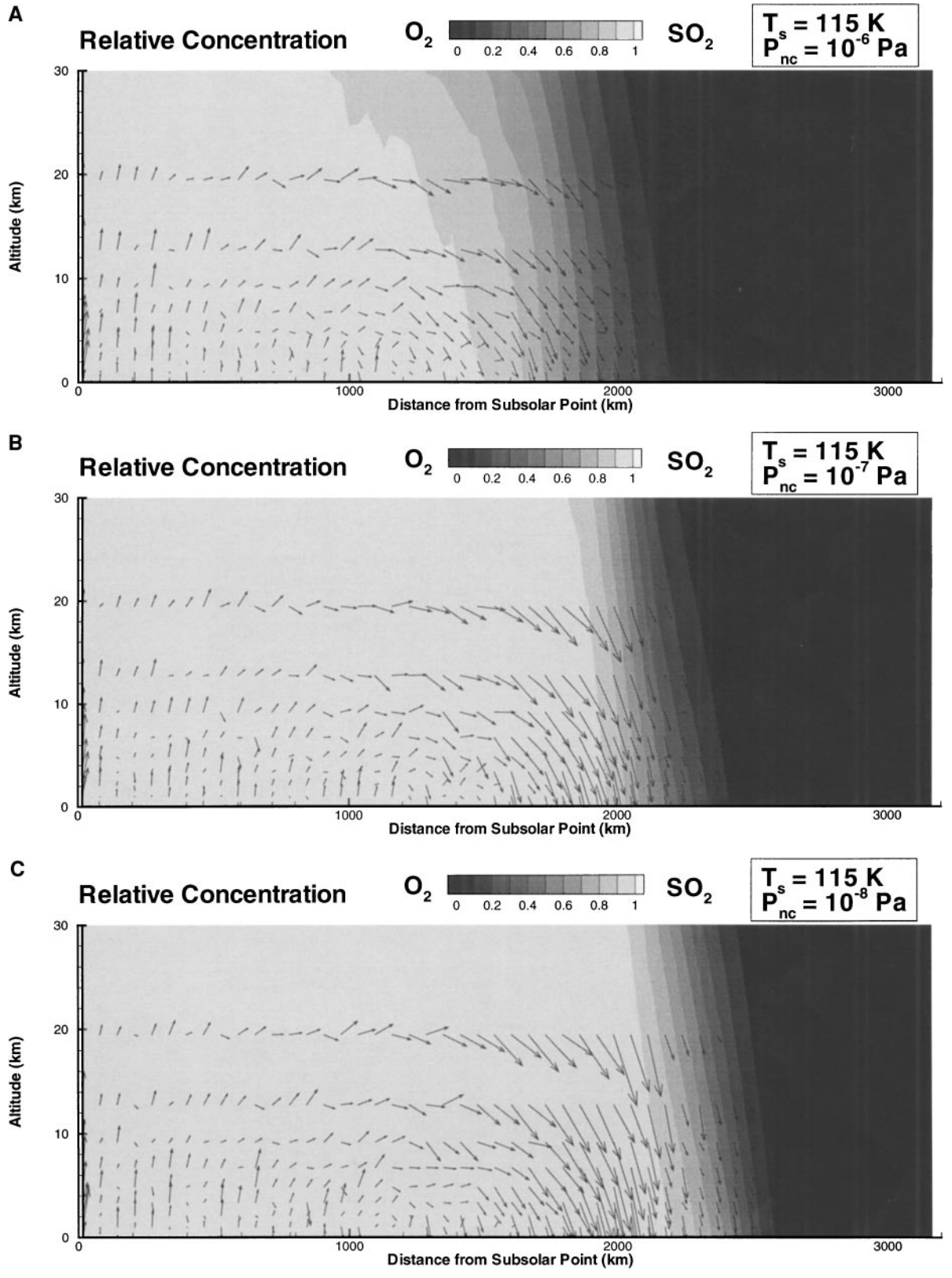

FIG. 8. Contours of the concentration of sulfur dioxide relative to oxygen with velocity vectors overlaid. The lightest areas represent 100% SO_2 (no O_2 molecules) and the darkest areas represent 100% O_2 (no SO_2 molecules). Shown are results for three pressures of noncondensible gas (O_2) on the night-side surface: (A) $P_{O_2} = 10^{-6}$ Pa, (B) $P_{O_2} = 10^{-7}$ Pa, (6) $P_{O_2} = 10^{-8}$ Pa.

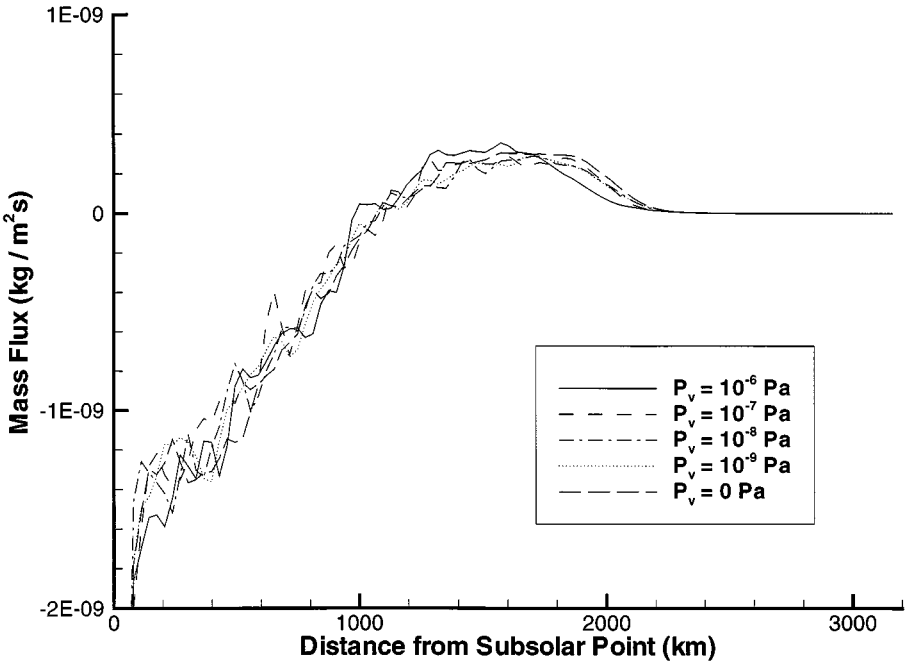

FIG. 9. Surface mass flux due to condensation/sublimation for several noncondensible gas pressures. As with Fig. 6, negative values denote flow out of the surface (sublimation) and positive values denote flow into the surface (condensation).

pattern. Only a back pressure of 10^{-6} Pa or greater produces any effect on the condensate distribution.

4. CONCLUSIONS

We have used a rarefied gas dynamics method for the simulation of large regions of the sublimation/condensation driven atmospheric flow on Io. Unlike inviscid models of Ingersoll (1989), Moreno *et al.* (1991), and Wong and Johnson (1995), our model indicates that a standing shock may form near the terminator. This is in common with the viscous models of Ingersoll *et al.* (1985) and Wong and Johnson (1996). The model presented better simulates the rarefied conditions which exist near the shock and also includes the full viscous terms; thus, it should more acurately predict the shock location and nature. We have admittedly made some large assumptions: we ignore planetary rotation, surface roughness, volcanos, three-dimensionality, and unsteadiness. We have not yet included effects of solar UV heating or dissociative chemistry and have only a crude model of non-LTE IR cooling in place—improvements are under way. Yet we have found some interesting features which may remain qualitatively unchanged as the simulations improve. We find:

1. The atmospheric flow is rarefied everywhere except near the surface in the subsolar region.
2. The bulk of the atmospheric boundary layer is likely laminar.
3. Atmospheric flow can produce highly oblique shock waves near the terminator.
4. The terminator shocks and/or plasma heating of the upper atmosphere produce a dramatically inflated and warmer upper atmosphere near the terminator.
5. There may be a range of surface frost deposition patterns which would be expected to result from the complex nature of the shock. These patterns can be indicative of the atmospheric gas dynamics.
6. The conveyor-belt-like nature of the SO_2 flow tends to push any modest noncondensible atmospheric species to the nightside behind an abrupt shock and species discontinuity. There appears to be little horizontal layering of the multi-species atmosphere.
7. For modest levels of background gas pressure there appears to be little influence on the SO_2 mass deposition rates, suggesting that (contrary to our initial expectations) such a gas would probably remain undetectable in the surface frost patterns.

ACKNOWLEDGMENTS

This research was supported by the Planetary Atmospheres program at NASA. Computational resources were provided in part by the Texas Advanced Computing Center.

REFERENCES

Austin, J. V., and D. B. Goldstein 1996. Direct numerical simulation of low-density atmospheric flow on Io. In *Molecular Physics and Hypersonic Flows* (M. Capitelli, Ed.), pp. 749–758. Kluwer Academic, Dordrecht/Norwell, MA.

Austin, J. V., and D. B. Goldstein 1997. Direct numerical simulation of Pluto's extended atmosphere. *Bull. Am. Astron. Soc.* **28**(3), 1079.

Austin, J. V., and D. B. Goldstein 1999. Simulation of supersonic rarefied atmospheric flows on Io. In *Rarefied Gas Dynamics* (R. Brun, R. Campargue, R. Gatignol, and J. C. Lengrand, Eds.), Vol. 2, pp. 681–688. Cepadues-Editions, Toulouse.

Ballester, G. E., D. F. Strobel, H. W. Moos, and P. D. Feldman 1990. The atmospheric abundance of SO_2 on Io. *Icarus* **88**, 1–23.

Ballester, G. E., M. A. McGrath, D. F. Strobel, X. Zhu, P. D. Feldman, and H. W. Moos 1994. Detection of the SO_2 atmosphere of Io with the Hubble space telescope. *Icarus* **111**, 2–17.

Bird, G. A. 1994. *Molecular Gas Dynamics and the Direct Simulation of Gas Flows*. Oxford Univ. Press. Oxford.

Chapman, S., and T. G. Cowling 1970. *The Mathematical Theory of Non-uniform Gases*, 3rd ed. Cambridge Univ. Press. Cambridge, UK.

Combi, M. R. 1996. Time-dependent gas kinetics in tenuous planetary atmospheres: The cometary coma. *Icarus* **123**, 207–226.

Hinson, D. P., A. J. Kliore, F. M. Flasar, J. D. Twicken, P. J. Schinder, and R. G. Herrera 1998. Galileo radio occultation measurements of Io's ionosphere and plasma wake. *J. Geophys. Res.* **103**, 29,343–29,352.

Ingersoll, A. P. 1989. Io meteorology: How atmospheric pressure is controlled locally by volcanos and surface frosts. *Icarus* **81**, 298–313.

Ingersoll, A. P., M. E. Summers, and S. G. Schlipf 1985. Supersonic meteorology of Io: Sublimation-driven flow of SO_2. *Icarus* **64**, 375–390.

Kliore, A. J., G. Fjeldbo, B. L. Seidel, D. N. Sweetnam, T. T. Sesplaukis, and P. M. Woiceshyn 1975. The atmosphere of Io from Pioneer 10 radio occultation measurements. *Icarus* **24**, 407–410.

Lellouch, E., M. Belton, I. de Pater, S. Gulkis, and T. Encrenaz 1990. Io's atmosphere from microwave detection of SO_2. *Nature* **346**, 639–641.

Lellouch, E., M. Belton, I. de Pater, G. Paubert, S. Gulkis, and T. Encrenaz 1992. The structure, stability, and global distribution of Io's atmosphere. *Icarus* **98**, 271–295.

Marconi, M. L., L. Dagum, and W. H. Smyth 1996. Hybrid fluid/kinetic approach to planetary atmospheres: An example of an intermediate mass body. *Astrophys. J.* **469**, 393–401.

McGrath, M. A., M. J. S. Belton, J. R. Spencer, and P. Satroretti 2000. Spatially resolved spectroscopy of Io's pele plume and SO_2 atmosphere. *Icarus* **146**, 476–493.

Moreno, M. A., G. Schubert, J. Baumgardner, M. G. Kivelson, and D. A. Paige 1991. Io's volcanic and sublimation atmospheres. *Icarus* **93**, 63–81.

Nelson, R. M., A. L. Lane, M. E. Morrill, B. D. Wallis, J. Gibson, W. D. Smythe, L. J. Horn, and B. J. Buratti 1993. The brightness of Jupiter's satellite Io following emergence from eclipse: Selected observations, 1981–1989. *Icarus* **101**, 223–233.

Pearl, J. C., R. Hanle, V. Kunde, W. Maguire, K. Fox, S. Gupta, C. Ponnamperuma, and F. Raulin 1979. Identification of gaseous SO_2 and new upper limits for other gases on Io. *Nature* **288**, 757–758.

Strobel, D. F., X. Zhu, and M. E. Summers 1994. On the vertical thermal structure of Io's atmosphere. *Icarus* **111**, 18–30.

Wong, M. C., and R. E. Johnson 1995. The effect of plasma heating on sublimation-driven flow in Io's atmosphere. *Icarus* **115**, 109–118.

Wong, M. C., and R. E. Johnson 1996. A three–dimensional azimuthally symmetric model atmosphere for Io. 1. Photochemistry and the accumulation of a nightside atmosphere. *J. Geophys. Res.* **101**, 23,243–23,254.

Wong, M. C., and W. H. Smyth 2000. Model calculations for Io's atmosphere at eastern and western elongations. *Icarus* **146**, 60–74.